# Effects of graphene nanoplatelets on the morphology of polycarbonate-graphene composite foams prepared by supercritical carbon dioxide two-step foaming

Gabriel Gedler[a], Marcelo Antunes[b] and José Ignacio Velasco[*]

Centre Català del Plàstic. Departament de Ciència dels Materials i Enginyeria Metal·lúrgica, Universitat Politècnica de Catalunya · BarcelonaTech (UPC), C/Colom 114, E-08222, Terrassa, Spain.

[a]gabriel.gedler@upc.edu, [b]marcelo.antunes@upc.edu and corresponding Author: [*]jose.ignacio.velasco@upc.edu; Phone: (+34)937837022; Fax: (+34)937841827

**Abstract.** Low density polycarbonate foams containing different amounts of graphene nanoplatelets with variable cellular morphologies were prepared using a supercritical carbon dioxide two-step foaming process, which consisted of the dissolution of supercritical $CO_2$ into moulded foam precursors and their later expansion by double contact restricted foaming. The effects of the processing conditions and graphene content on the cellular morphology of the obtained foams were investigated, showing that the addition of increasingly higher amounts of graphene nanoplatelets resulted in foams with increasingly smaller cell sizes and higher cell densities, due on the one hand to their effectiveness as cell nucleating agents and on the other to their platelet-like geometry, which limited $CO_2$ loss during foaming due to a barrier effect mechanism. Especially significant was the addition of 5 wt% graphene nanoplatelets, as the high concentration of graphene limited $CO_2$ escape and cell coalescence during expansion, enabling to obtain highly expanded microcellular foams.

**Keywords:** polycarbonate foams, graphene nanoplatelets, supercritical carbon dioxide, two-step foaming.

## 1. Introduction

Graphene-filled polymer foams have recently aroused a great interest in the scientific and industry communities [1-4], as the incorporation of graphene can dramatically enhance the electrical, physical, mechanical and barrier properties of polymers at extremely low loadings and, as a consequence, extend their potential applications to fields such as electronics, aerospace, automotive, green energy, among others [5]. The use of supercritical carbon dioxide ($scCO_2$) dissolved into a given polymer has become one of the most common strategies used to prepare graphene-filled polymer foams [2-4,6]. Carbon dioxide acts as polymer plasticizer, decreasing its glass transition temperature and facilitating expansion due to decreased polymer viscosity [7], in some cases even leading to cell coalescence and as a result to a decrease in cell density [8]. Thus, foaming processing conditions play an essential role in the final morphological/microstructural characteristics of the resulting foams. On the other hand, several studies have indicated that a small amount of well-dispersed nanoparticles can act as cell nucleation sites and that nucleation efficiency is dependent on particle size, shape, surface properties and dispersion quality [2,4,9]. In addition, it has been shown that the combination of graphene nanoplatelets and $scCO_2$ during foaming may have remarkable effects on the microstructure of the developed foams [10].

It is known that polymer foaming using carbon dioxide in supercritical conditions can be done in one [11-12] or two steps [13-15] inside high pressure vessels. In the case of one-step foaming, $CO_2$ dissolution, expansion and cooling of samples takes place inside the high pressure vessel, while in two-step foaming the expansion stage can be done either inside the same vessel used to initially dissolve the carbon dioxide or outside by heating the $CO_2$-saturated samples using an oil bath [16] or a hot-press [15]. Particularly, graphene-filled polycarbonate foams have been prepared by both one-step [6] as well as two-step foaming [17]. Process conditions applied during foaming are crucial regarding the morphology of the developed foams, possible polymer microstructural changes and graphene dispersion. In this sense, Ma et al. [17] have reported the effective

heterogeneous cell nucleation effect of graphene, with an increase in graphene content promoting the formation of foams with increasingly smaller cell sizes.

Following a previous work that considered the effects of foaming parameters, particularly $CO_2$ dissolution temperature and foaming heating time conditions, on the cellular morphology of unfilled PC foams prepared by two-step foaming [15], this paper pretends to extend the study to the effects of the addition of variable concentrations of graphene nanoplatelets. Based on the amount of added graphene nanoplatelets and particular interaction with $scCO_2$ used in foaming it was possible to prepare foams with tailored cellular structures that varied from isotropic-like microcellular to foams with larger an elongated cells, opening up a broader range of applications for these lightweight materials.

## 2. Experimental

### *2.1. Compounding and moulding of foam precursors*

Polycarbonate (Lexan-123R-PC), supplied by Sabic in the form of pellets, with a density of 1.2 $g/cm^3$ and melt flow index (MFI) of 17.5 dg/min, measured at 300 ºC and 1.2 kg, was melt-compounded with 0.5 and 5 wt% of graphene nanoplatelets (GnP) using a Brabender Plasti-Corder static mixer. The graphene nanoplatelets used in this study (xGnP-M-15) were supplied by XG Sciences, Inc. These nanoplatelets were 6 to 8 nm thick with a 15 μm average diameter and a density of 2.2 $g/cm^3$, as reported by the manufacturer. The graphene-filled PC composites were prepared by placing the previously physically mixed components inside the Brabender mixer for 2 min at 180 ºC using a constant rotating screw speed of 30 rpm. The rotating speed was then increased to 60 and 120 rpm for 1 and 3 min, respectively. Afterwards, each composite was pelletized, quickly transferred into a circular-shaped mould and compression-moulded at 220 ºC and 45 bar in a hot-plate press (IQAP LAP PL-15) to circular-shaped plates with a thickness of 3.5 mm and diameter of 74 mm following the procedure explained in a previous work [6]. The plates

obtained at the end of this stage were used as foam precursors. The samples used for the $CO_2$ desorption experiments were directly cut from these plates to a typical diameter value of 40 mm.

*2.2. Foaming process: Stage I - Supercritical carbon dioxide dissolution*

The foam precursors were placed inside a high pressure vessel (Büchiglasuster kiloclave), where supercritical carbon dioxide ($scCO_2$) was initially dissolved. Two $scCO_2$ dissolution temperatures were considered: 80 and 100 ºC, in both cases applying a dissolution time of 210 min. The $scCO_2$ was initially introduced in the vessel at 70 bar, reaching a final dissolution pressure of 140 and 180 bar, respectively for 80 and 100 ºC. Once carbon dioxide was dissolved into the foam precursors, these were cooled down to room temperature by re-circulating water through the vessel's cooling jacket while keeping the vessel pressurized at 15 ºC/h in order to avoid undesirable pre-foaming. After slow depressurization at room temperature of the remaining $scCO_2$ (average rate of depressurization: 3 bar/min), the foam precursors containing $CO_2$ were taken out from the vessel and left to stabilize at room temperature and atmospheric pressure for 120 min prior to Stage II (see Fig. 1).

*2.3. Foaming process: Stage II - Double contact restricted foaming*

The foam precursors with $CO_2$ stabilized at the end of Stage I were once again placed in the circular-cavity mould and foamed in the hot-plate press at 165 ºC applying a constant pressure of 60 bar. The circular-cavity mould and metal plates used in this stage were pre-heated at 165 ºC prior to positioning of the precursors and foaming. The double contact restricted foaming used in this stage guaranteed the homogeneous heating of the precursors and ensured flatness of the surfaces for later characterization. After applying a heating time that varied between 40 and 100 s, the applied pressure was abruptly released, allowing the foam precursors with $CO_2$ to grow in both vertical and width directions (VD and WD, respectively). After the expansion, the obtained foams were quickly removed from the plates and left to cool at room temperature by direct contact with air (see Fig. 1).

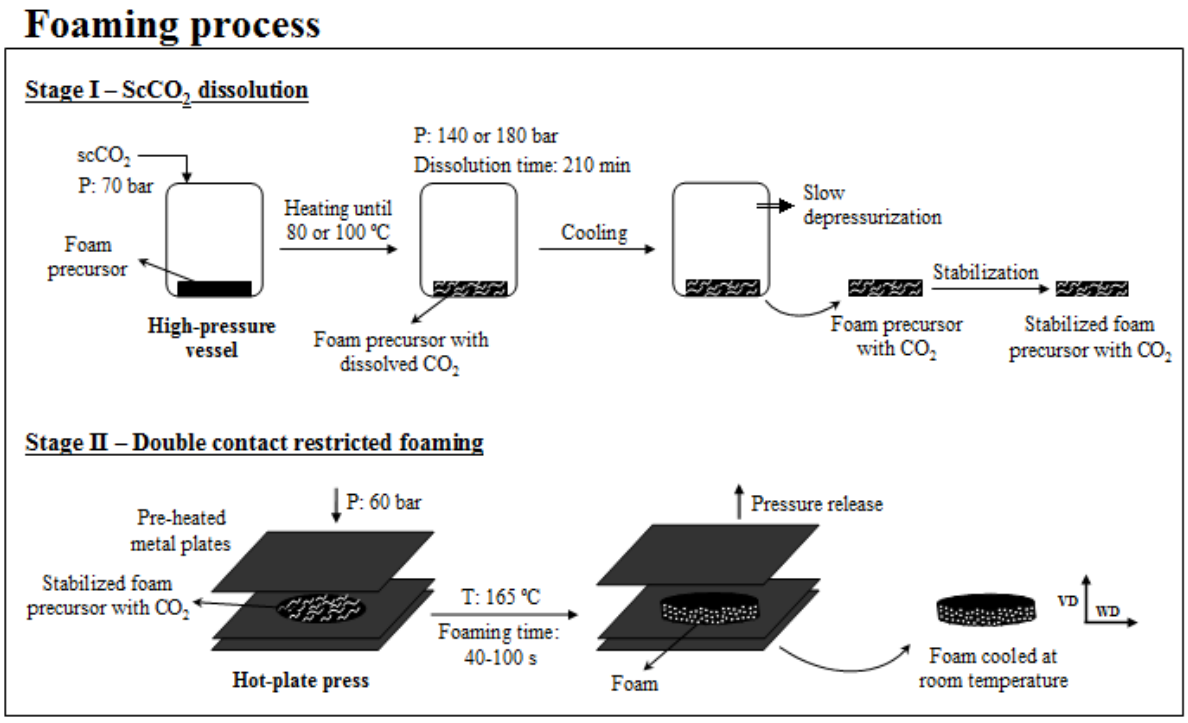


**Fig. 1.** Scheme of the $scCO_2$ two-step foaming process.

*2.4. $CO_2$ desorption experiments*

Desorption experiments were carried out in order to measure the $CO_2$ diffusion coefficient in the graphene-filled PC composites for the two different dissolution temperatures. The samples used in these experiments were obtained from the foam precursors by reducing their diameter to 40 mm. After applying the conditions already indicated in Stage I, samples were cooled down to room temperature, removed from the vessel and quickly transferred to a balance in order to record the evolution of $CO_2$ mass loss as a function of desorption time (see scheme presented in Fig. 2).

The maximum concentration of $CO_2$ in the samples after decompression ($M_0$) was calculated by extrapolating to zero desorption time following the initial slope method [18]. The sorption and desorption of gases out of or into polymers may be assumed to be Fickian-like, the diffusion behavior being described by [19]:

$$\frac{M_t}{M_0} = 1 - \sum_{n=0}^{\infty} \frac{8}{(2n+1)^2 \pi^2} \exp\left(-\frac{D(2n+1)^2 \pi^2 t}{l^2}\right) \quad (1)$$

For short desorption time periods and assuming one-dimensional through-plane diffusion, the $CO_2$ desorption diffusion coefficient ($D_d$) can be determined by plotting $M_t/M_0$ as a function of $t/l^2$, where $M_t$ is the $CO_2$ concentration at time $t$ and $l$ is the thickness of the sample, according to the following equation [20]:

$$\frac{M_t}{M_0} = 1 - \frac{8}{\pi^2}\exp\left(-\frac{D_d t}{l^2}\right) \tag{2}$$

The $CO_2$ diffusion coefficient was determined from the slope of the $M_t/M_0$ vs. $t/l^2$ curve taking into account the last data range and the value of $M_0$.

Equations and assumptions used for determining $D_d$ have been schematically summarized in Fig. 2.

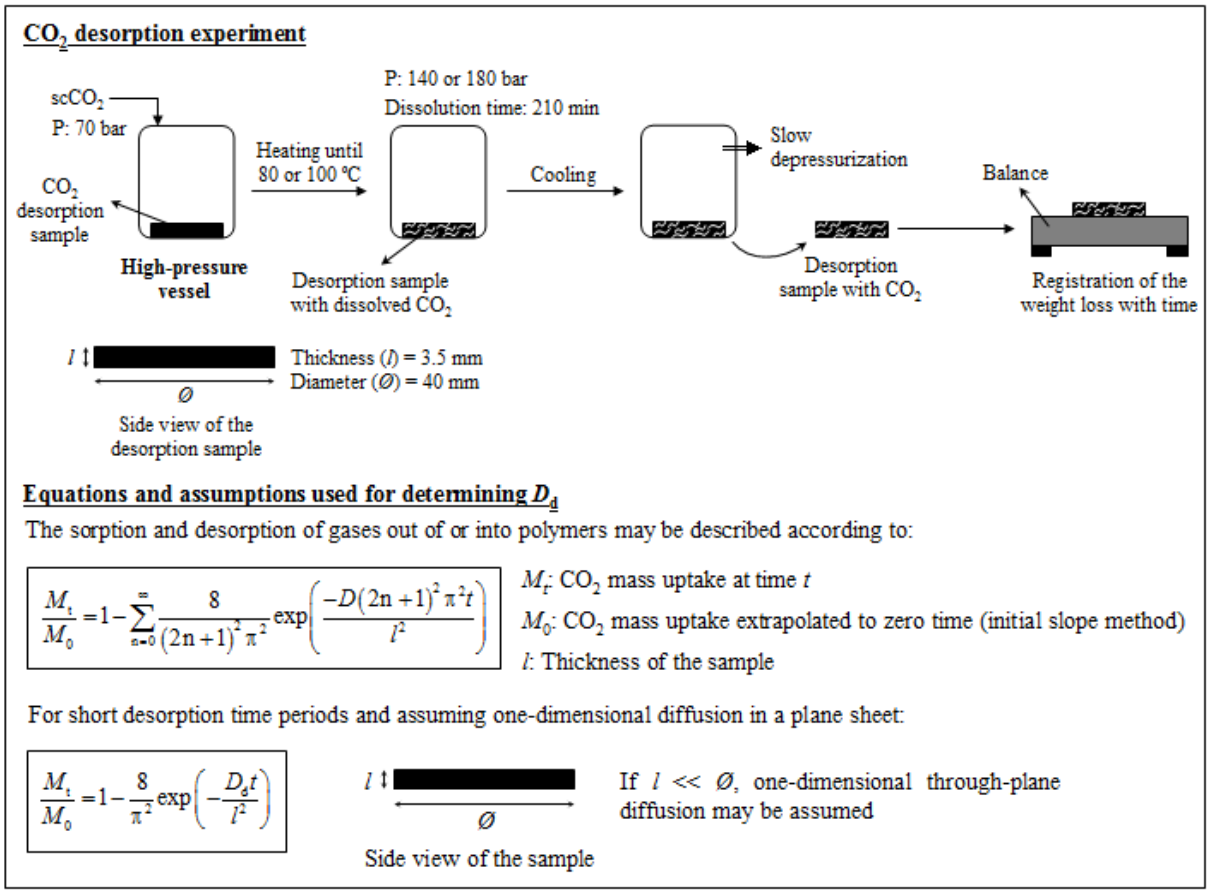


**Fig. 2.** Scheme of the $CO_2$ desorption experiment and equations used for determining $D_d$.

*2.5. Cellular structure characterization*

The density of foams was measured following standard procedures (ISO 845), while the relative density was calculated by dividing this value by the density of the respective foam precursor. Scanning electron microscopy (SEM) was used to analyze the cellular structure of the foams. Samples were frozen in liquid nitrogen and then fractured. The fracture surface was sputter-coated with a thin layer of gold in an argon atmosphere using a BAL-TECSCD005 Sputter Coater. Micrographs were obtained using a JEOL JSM-5610 microscope applying a voltage of 10 kV and a working distance of 40 mm.

The average cell size in the vertical ($\phi_{VD}$) and width ($\phi_{WD}$) foaming directions were measured using the intercept counting method [21]. The cell aspect ratio (*AR*) was determined by dividing the value of the average cell size in the vertical direction by that measured in the horizontal one ($AR = \phi_{VD}/\phi_{WD}$). The cell nucleation density ($N_f$) was calculated according to:

$$N_f = \left(\frac{n}{A}\right)^{3/2}\left(\frac{\rho_s}{\rho_f}\right) \quad (3)$$

where $n$ is the number of cells per area $A$ of micrograph (in $cm^2$) and $\rho_s$ and $\rho_f$ are, respectively, the solid and foam densities.

*2.6. X-ray diffraction analysis*

X-ray diffraction (XRD) was carried out using a Panalytical diffractometer in order to observe any possible crystal structure modifications of PC and graphene nanoplatelets after melt-compounding and foaming. CuKα radiation ($\lambda = 1.54$ Å) was used in the measurements, with the diffractometer operating at room temperature at 40 kV and 40 mA, scanning from 2 to 60º using a step of 0.02º. Samples were prepared by cutting 20 mm × 20 mm squares, with a typical thickness

below 5.0 mm in the case of foams, making sure to remove the solid outer skins generated during foaming. In the case of the unfoamed samples, 3.2 mm thick squared samples were used.

## 3. Results and discussion

### *3.1. Influence of the dissolution temperature on the $CO_2$ desorption kinetics*

The dissolution of $scCO_2$ in the graphene-filled PC composites at 80 ºC resulted in a maximum concentration of dissolved $CO_2$ ($M_0$) of 54.1 and 32.0 mg of $CO_2$/g of composite, respectively for a GnP concentration of 0.5 and 5 wt%. This important decrease with increasing the amount of GnP could be attributed to a physical barrier effect promoted by the graphene nanoplatelets, making it harder for $CO_2$ to enter the composite. Also, it was observed that it was possible to dissolve a higher concentration of $CO_2$ in the composite with increasing $CO_2$'s dissolution temperature, from the 32.0 mg of $CO_2$/g of composite at 80 ºC to 40.5 mg of $CO_2$/g of composite at 100 ºC for composites containing 5 wt% GnP, which was related to a higher molecular mobility of PC in said conditions.

The $CO_2$ desorption curves displayed in Fig. 3 show the evolution of the $CO_2$ concentration present in the several graphene-filled PC composites with time for the two considered $CO_2$ dissolution temperatures. Assuming a desorption behavior according to Eq. (2) (see curve fits embedded in Fig. 3), graphene-filled PC composites with $CO_2$ dissolved at 80 ºC presented values of the $CO_2$ diffusion coefficient ($D_d$) of $6.75 \times 10^{-12}$ $m^2/s$ (0.5 wt% GnP) and $5.99 \times 10^{-12}$ $m^2/s$ (5 wt% GnP), while those with $CO_2$ dissolved at 100 ºC showed diffusion coefficients of $3.34 \times 10^{-12}$ $m^2/s$ (0.5 wt% GnP) and $3.01 \times 10^{-12}$ $m^2/s$ (5 wt% GnP). As can be seen, as the higher dissolution temperature induced a larger quantity of $CO_2$ dissolved in the composites due to the higher molecular mobility of PC promoted by the plasticizing effect of $CO_2$, the resulting diffusion coefficients resulted smaller, suggesting that this higher PC mobility could promote the formation of ordered PC structures and/or a better dispersion of the graphene nanoplatelets, enhancing the barrier effect of these composites. Nevertheless, as will be shown later on by XRD analysis, the several graphene-filled PC composite foams resulted fully amorphous (see section 3.3).

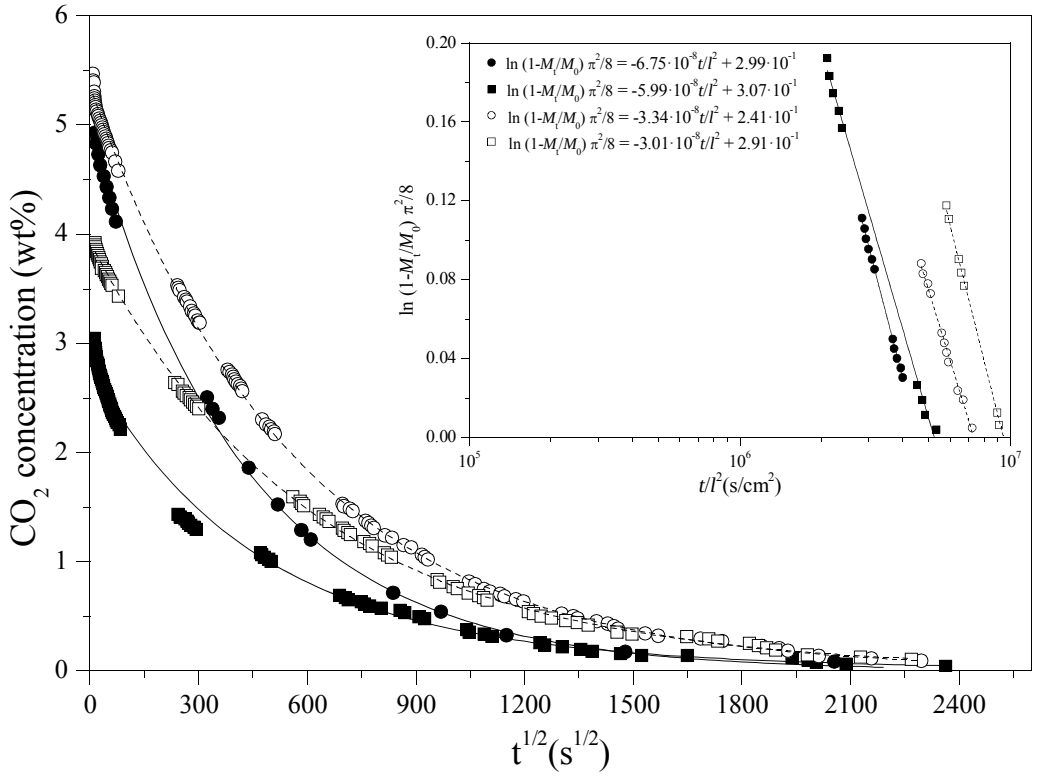


**Fig. 3.** $CO_2$ desorption curves for graphene-filled PC composites with $CO_2$ dissolved at 80 ºC: 0.5 wt% GnP (filled circles) and 5 wt% GnP (filled squares) and 100 ºC: 0.5 wt% GnP (hollow circles) and 5 wt% GnP (hollow squares). Embedded in the figure are the curve fits used to determine $D_d$ for each composite according to Eq. (2).

*3.2. Influence of the heating time on the cellular structure*

As can be seen by the micrographs presented in Figs. 4a and b, the typical cellular morphology of PC composite foams containing 0.5 wt% GnP prepared by dissolving $CO_2$ at 80 ºC can be divided in two different parts, in a similar way as the unfilled PC foams studied in a previous work [15]: an isotropic-like homogeneous microcellular structure formed towards the centre of the sample, which represented the main and dominant cellular morphology of the foams obtained by dissolving $CO_2$ at 80 ºC, and a second part found near the upper and lower foam skins characterized by bigger cells.

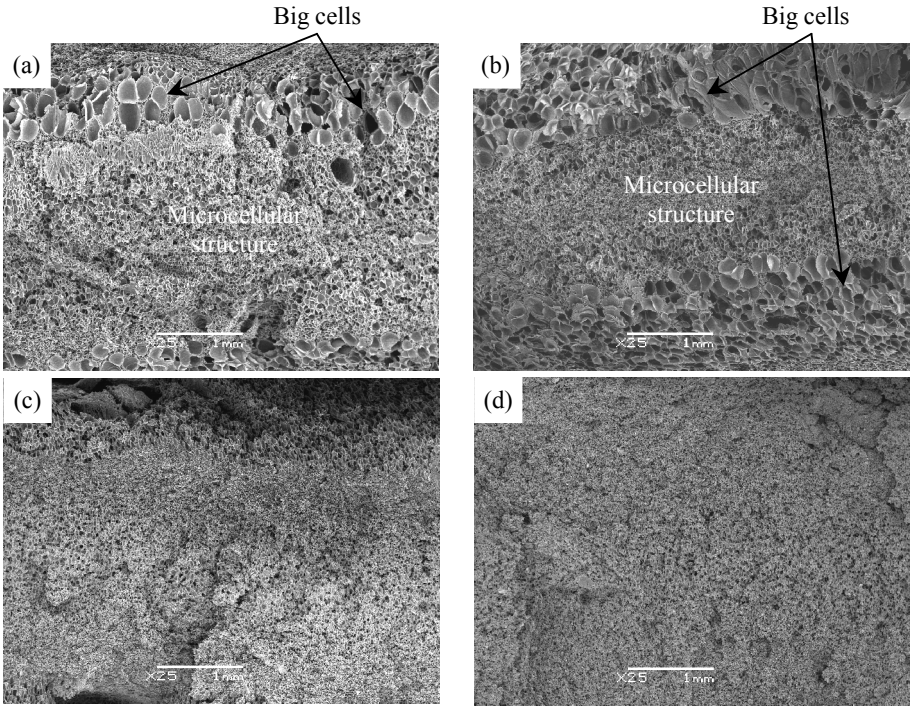


**Fig. 4.** Micrographs showing the typical cellular morphology of graphene-filled PC composite foams prepared by dissolving $CO_2$ at 80 ºC: 0.5 wt% GnP (a) 40 s and (b) 100 s and 5 wt% GnP (c) 40 s and (d) 100 s of heating time applied during Stage II.

For this set of foams, the microcellular structure was formed as a result of a proper combination of $CO_2$ dissolution conditions (Stage I) and sudden pressure release after heating while restraining the expansion (Stage II). The formation of the larger cells was attributed to a non-uniform heat transfer at the end of Stage II, with the material remaining hotter at the surface due to direct contact with the metal plates used to restrict the expansion, promoting cell coalescence.

As the main cellular morphology of PC composite foams containing 0.5 wt% GnP prepared by dissolving $CO_2$ at 80 ºC was that corresponding to a microcellular-like structure, the cellular characterization analysis for these foams was carried out in this zone. Table 1 summarizes the main results of this analysis, indicating the average cell sizes in both VD and WD directions, cell nucleation density and cell aspect ratio.

Table 1. Cellular structure characterization results of PC foams containing 0.5 wt% GnP prepared by dissolving $CO_2$ at 80 ºC.

| Heating time (s) | Relative density | $\phi_{VD}$ (μm) | $\phi_{WD}$ (μm) | $N_f$ (cells/cm$^3$) | *AR* |
|---|---|---|---|---|---|
| 40 | 0.14 | 26 ± 3 | 21 ± 2 | $6.07 \times 10^8$ | 1.3 |
| 60 | 0.19 | 46 ± 4 | 34 ± 3 | $6.19 \times 10^7$ | 1.4 |
| 80 | 0.24 | 20 ± 2 | 14 ± 1 | $7.88 \times 10^8$ | 1.4 |
| 100 | 0.28 | 12 ± 1 | 11 ± 1 | $1.56 \times 10^9$ | 1.1 |

For these foams, which globally displayed a cellular morphology characterized by micrometric-sized cells slightly oriented in the vertical foam growth direction ($AR > 1$), the highest average cell sizes were observed when they were prepared by heating in Stage II during 60 seconds. Nevertheless, the highest value of the expansion ratio, defined as the quotient between the density of the foam and that of the solid material, i.e., the reciprocal of relative density, was 6.9 for PC + 0.5 wt% GnP composite foams prepared by heating during 40 seconds, which can be explained by the presence of a fraction of larger cells that influenced the estimation of the expansion ratio.

It is evident that the heating time applied during Stage II played a main role in the cellular morphology of these composite foams, as for heating times between 40 and 60 seconds cell sizes increased with increasing time, while for longer times (80 and 100 seconds) cell sizes decreased. Particularly, the reduction of the cell sizes after 60 seconds of heating time can be explained as a restriction in the flow of material at the moment of expansion, meaning a possible change in the microstructure of PC and/or orientation of graphene nanoplatelets before and during the early stages of foaming, which could interact with PC molecules restraining material stretching during cell growth.

This cellular morphology characterized by the simultaneous presence of micrometric-sized cells and considerably larger cells disappeared for PC composite foams containing 5 wt% GnP (see Figs. 4c and d), which only displayed a microcellular structure, attributed on the one hand to a higher cell

nucleating effect promoted by the graphene nanoplatelets and on the other to a more effective physical barrier effect of said nanoplatelets, inhibiting $CO_2$ loss during foaming, the combination of which leading to composite foams with homogeneous cellular structures and significantly smaller cell sizes.

The cellular morphology evolution with heating time applied during Stage II of foaming of PC composite foams containing 0.5 and 5 wt% GnP prepared by dissolving $CO_2$ at 80 ºC is summarized in Fig. 5. Both unfilled PC foams as well as PC composite foams containing 0.5 wt% GnP reached a maximum cell size for a heating time between the two considered limits of 40 and 100 seconds, although foams containing 0.5 wt% GnP reached this maximum much earlier. While this maximum was observed at 100 seconds for the unfilled PC foams, for PC foams containing 0.5 wt% GnP it was reached at 60 seconds. This behavior could be attributed to the interaction between graphene nanoplatelets and PC molecules in the presence of $CO_2$ [10].

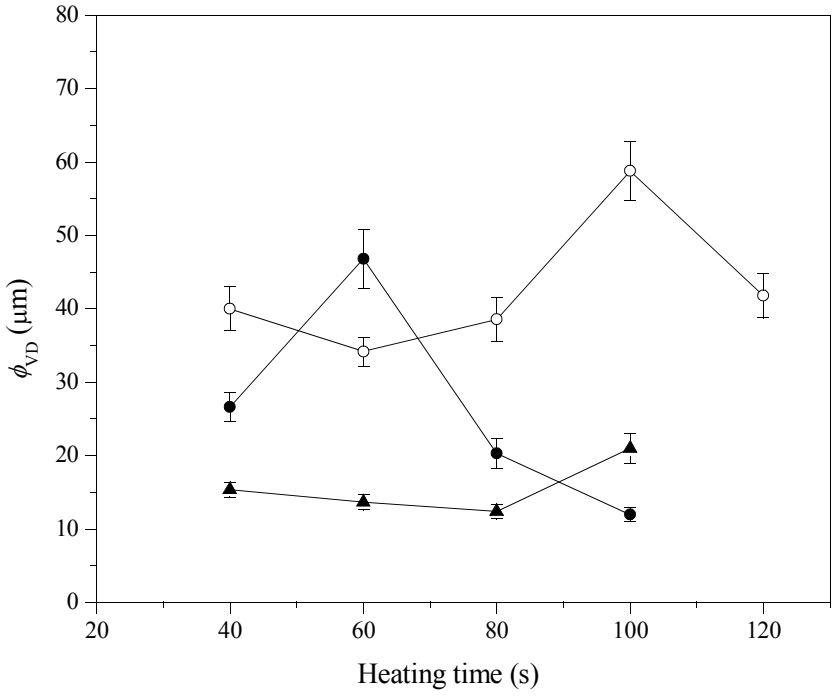


**Fig. 5.** Evolution of the average cell size with the heating time applied during Stage II of foaming for foams prepared by dissolving $CO_2$ at 80 ºC: unfilled PC foams (hollow circles) [15], PC

composite foams containing 0.5 wt% GnP (filled circles) and PC composite foams containing 5 wt% GnP (filled triangles).

For PC composite foams containing 5 wt% GnP it seems that this behavior does not take place within the range of considered heating times, possibly due to the fact that the nucleation effect promoted by the high quantity of GnP nanoplatelets takes over the possible stretch-induced order in PC. It has previously been reported that the stretching of polymer molecules due to shear promotes polymer ordering [22-25].

*3.3. Influence of the dissolution temperature on the cellular structure*

While a temperature of $CO_2$ dissolution in Stage I of 80 ºC ultimately resulted in graphene-filled PC composite foams with a characteristic microcellular structure (see Fig. 4), PC + 0.5 wt% GnP foams prepared by dissolving $CO_2$ at 100 ºC presented a cellular morphology with bigger and VD-elongated cells with increasing the heating time in Stage II, as can be seen by the micrographs displayed in Fig. 6. This cellular structure resulted from cell coalescence, which became dominant after a heating time of 60 seconds. Despite the presence of cell coalescence, a remarkable cell size reduction was observed when comparing these foams with the unfilled PC foams prepared under similar conditions [15], which was attributed to the effective cell nucleating effect promoted by the graphene nanoplatelets.

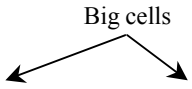

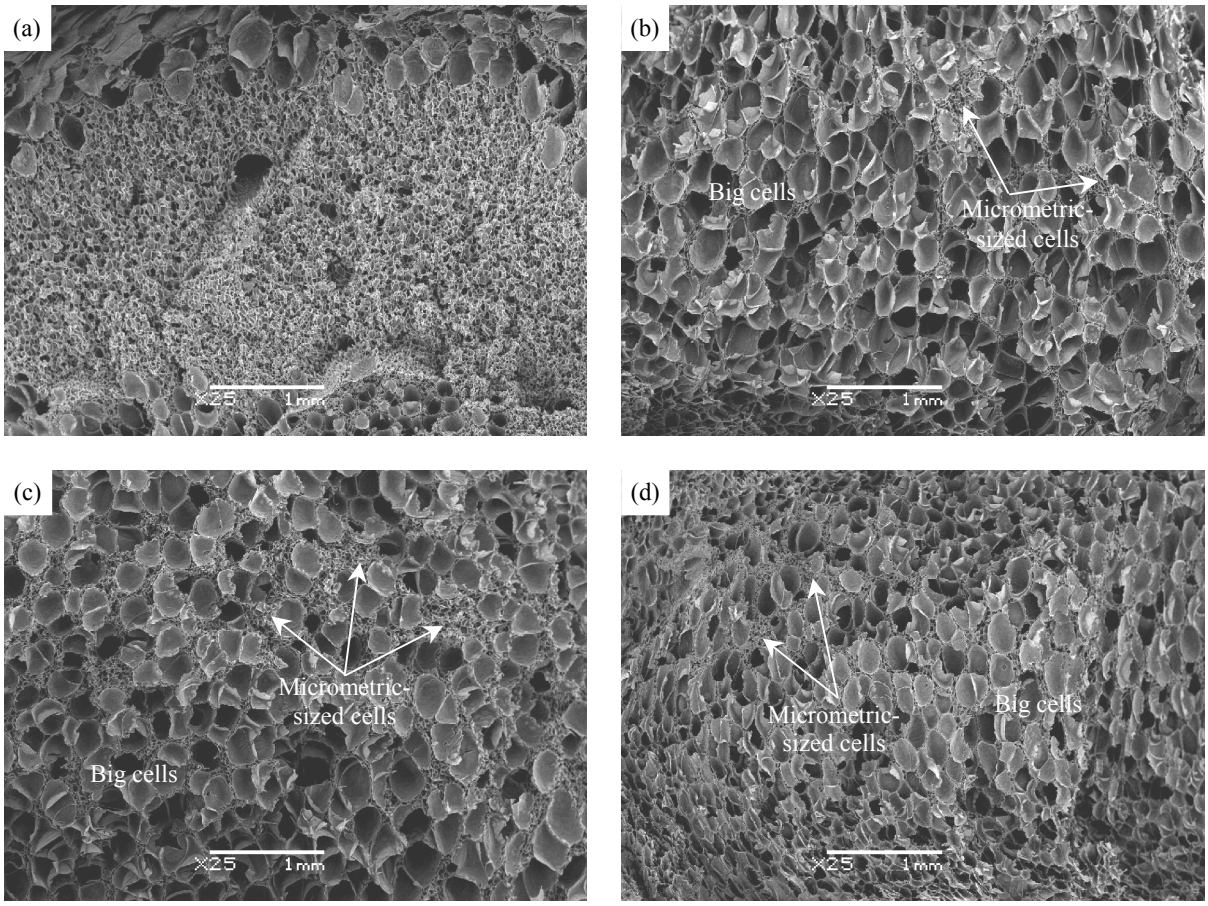


**Fig. 6.** Micrographs showing the typical cellular morphology of PC composite foams containing 0.5 wt% GnP prepared by dissolving $CO_2$ at 100 ºC: (a) 40 s, (b) 60 s, (c) 80 s and (d) 100 s of heating time applied during Stage II.

PC + 0.5 wt% GnP composite foams prepared by dissolving $CO_2$ at 100 ºC and applying a heating time during Stage II of 40 seconds presented a cellular morphology characterized on the one hand by a characteristic microcellular structure similar to that of the composite foams obtained by dissolving $CO_2$ at 80 ºC (cell sizes around 25 μm) and on the other by an area with bigger and slightly elongated cells in the vertical foam growth direction. As can be seen in Figs. 6b, c and d, for heating times higher than 40 seconds these foams presented cellular structures mainly formed by these bigger and elongated cells (cell sizes around 200 μm and cell aspect ratios around 1.6).

As can be seen by the evolution of the average cell sizes of unfilled and graphene-filled PC foams with the heating time applied during Stage II presented in Fig. 7, the increment of GnP

concentration promoted the formation of foams with significantly lower average cell sizes. Particularly noticeable are the differences between foams when applying a heating time of 100 seconds, with the addition of only 0.5 wt% GnP leading to a reduction in cell size of around 70% and respective cell nucleation density increase when compared to the unfilled PC foams. More spectacular was the cell size reduction when adding 5 wt% GnP, with these foams presenting a characteristic microcellular structure with cell sizes around 10 μm and cell densities > $10^9$ cells/$cm^3$. Also important is the fact that it was possible to obtain both unfilled as well as graphene-filled PC foams with microcellular morphologies for short heating times (40 seconds of heating time applied during Stage II).

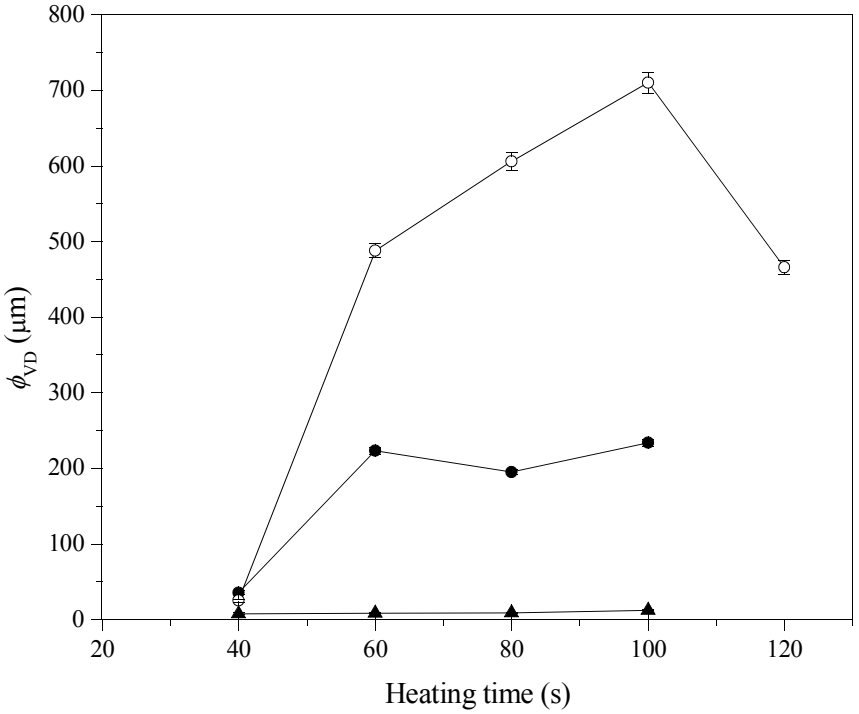


**Fig. 7.** Evolution of the average cell size with the heating time applied during Stage II of foaming for foams prepared by dissolving $CO_2$ at 100 ºC: unfilled PC foams (hollow circles) [15] , PC composite foams containing 0.5 wt% GnP (filled circles) and PC composite foams containing 5 wt% GnP (filled triangles).

The cellular structure differences between PC composite foams containing 0.5 wt% GnP prepared by dissolving $CO_2$ at 80 and 100 ºC were attributed to the amount of $CO_2$ present in the foam precursors just before placing them in the press for foaming in Stage II, i.e. 3.8 wt% $CO_2$ in the case of 80 ºC and 4.3 wt% in the case of 100 ºC. The higher amount of $CO_2$ present in PC + 0.5 wt% GnP foam precursors prepared by dissolving $CO_2$ at 100 ºC seemed to promote cell coalescence for heating times higher than 40 seconds, ultimately resulting in lower cell nucleation densities (see Fig. 8). On the contrary, when the concentration of GnP was increased to 5 wt% not only no cell coalescence was observed but in fact the combination of a higher $CO_2$ concentration as well as an effective cell nucleation effect favored by the high concentration of GnP nanoplatelets promoted the formation of foams with reduced cell sizes and hence increased cell densities.

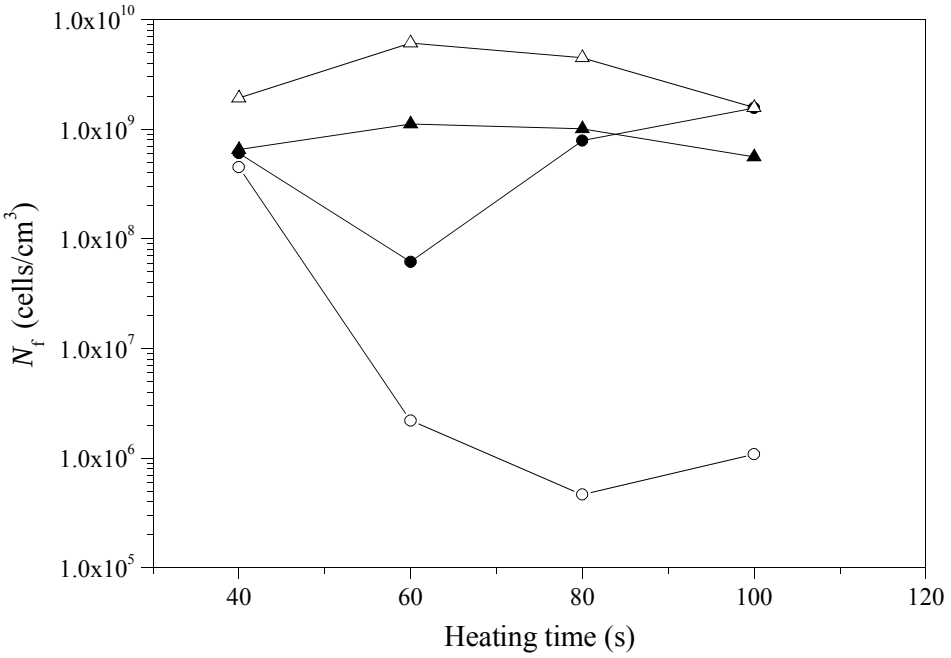


**Fig. 8.** Evolution of the cell nucleation density with the heating time applied during Stage II of foaming for foams prepared by dissolving $CO_2$ at 80 ºC: PC composite foams containing 0.5 wt% GnP (filled circles) and PC composite foams containing 5 wt% GnP (filled triangles) and by dissolving $CO_2$ at 100 ºC: PC composite foams containing 0.5 wt% GnP (hollow circles) and PC composite foams containing 5 wt% GnP (hollow triangles).

The analysis of the effects of the addition of different concentrations of graphene nanoplatelets on the morphology of PC foams made possible a better understanding of how to use the foaming conditions in order to develop low density PC composite foams with variable cellular structures, from isotropic-like microcellular foams (cell sizes from 5 to 60 μm) to foams with larger and elongated cells (see Fig. 9).

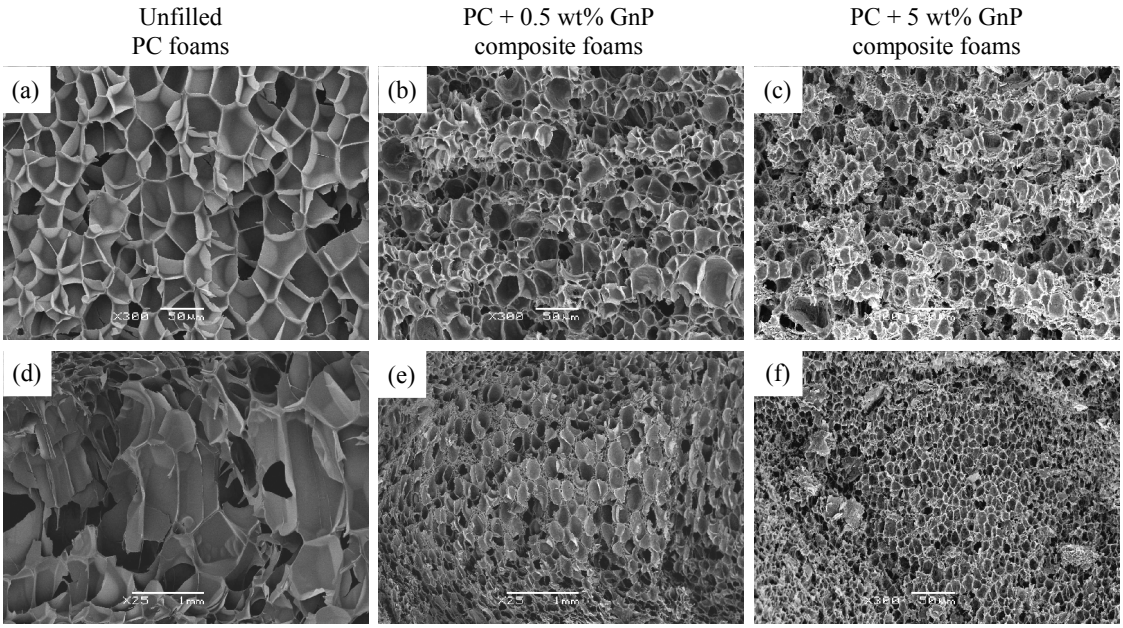


**Fig. 9.** Micrographs showing different cellular morphologies that can be achieved by controlling foaming process conditions and graphene content: (a-c) $CO_2$ dissolution temperature of 80 ºC and (d-f) $CO_2$ dissolution temperature of 100 ºC.

It needs to be pointed out that the several graphene-filled PC composite foams prepared by $scCO_2$ two-step foaming resulted fully amorphous according to XRD. This is one of the main differences from the PC-graphene composite foams prepared by one-step foaming already analyzed in a previous work [10] that showed the development of PC crystals by both XRD as well as by differential scanning calorimetry (DSC). Said crystallinity was attributed to the noticeable higher temperatures used for dissolving $scCO_2$ in the one-step foaming process (> 200 ºC) when compared

with the temperatures used for dissolving $scCO_2$ in two-step foaming (80 and 100 ºC). These higher temperatures allowed an easier rearrangement of PC molecules into a more favorable energy state, promoting their crystallization and ordering, as already discussed in our previous work [10]. As from the selected foaming conditions the highest $scCO_2$ dissolution temperature (100 ºC) was the one that favored the highest possible molecular mobility of PC in the graphene-filled PC composites and thus the most favorable conditions for PC crystallization, these foams were the ones analyzed by XRD. As can be seen by the spectra presented in Fig. 10, no crystalline diffraction peaks associated to PC crystallization were observed, with the characteristic amorphous halo of PC appearing at around 17.5º. Besides PC's amorphous halo, only the characteristic (002) diffraction peak typical of graphitic-like structures such as GnP found at around 26.5º appeared in all composites, in the particular case of PC + 0.5 wt% GnP foams as a peak of reduced intensity due to the considerably lower effective concentration of GnP nanoplatelets (see arrows embedded in Fig. 10).

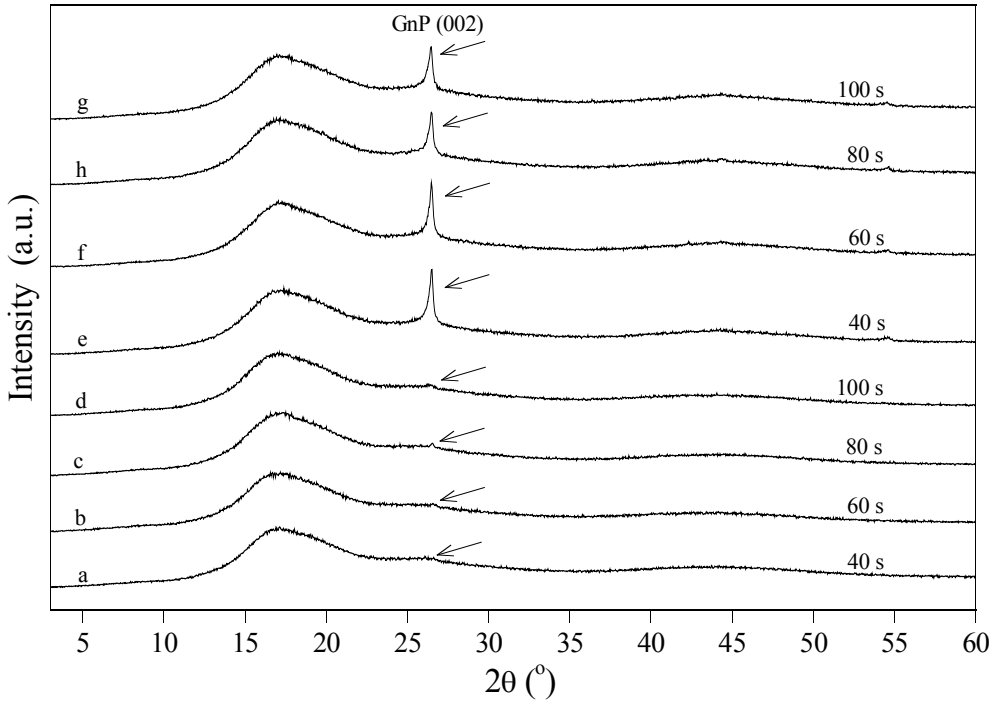

**Fig. 10.** X-ray diffraction spectra of graphene-filled PC composite foams prepared by dissolving $CO_2$ at 100 ºC: (a-d) 0.5 wt% GnP and (e-h) 5 wt% GnP.

Note: Heating times applied during Stage II are indicated for each spectrum.

## 4. Conclusions

It was possible to prepare low density graphene-filled PC composite foams with variable morphologies from microcellular-like to cellular structures characterized by large elongated cells using a two-step foaming process that consisted of the dissolution of $scCO_2$ into previously moulded foam precursors and their later expansion by double contact restricted foaming.

Although the maximum concentration of $CO_2$ dissolved in the composites during the first stage of foaming significantly decreased with increasing the amount of GnP, which was attributed to a physical barrier effect of the nanoplatelets to $CO_2$ entrance, this could be counteracted by increasing the dissolution temperature, related to a higher PC molecular mobility at higher temperature.

PC foams with 0.5 wt% GnP prepared by dissolving $CO_2$ at 80 ºC presented an isotropic-like microcellular structure with larger cells resulting from cell coalescence near the foam skins, attributed to a non-uniform heat transfer due to direct contact with the metal plates used to restrict the expansion. For short heating times the average cell size increased with increasing time, while for longer times cell size decreased, related to a restriction in material flow during expansion. On the other hand, PC foams containing 5 wt% GnP displayed a full microcellular morphology with considerably smaller cell sizes resulting from the combination of a higher cell nucleating effect promoted by the higher amount of GnP and a more effective physical barrier effect of said nanoplatelets, inhibiting $CO_2$ escape during foaming.

As $CO_2$ dissolution temperature increased to 100 ºC, the morphology of PC foams with 0.5 wt% GnP evolved to a cellular structure formed by increasingly bigger and oriented cells with increasing the heating time. However, these foams still presented an important cell size reduction and cell density increase regarding the unfilled foams prepared at similar conditions. More spectacular was

the cell size reduction when adding 5 wt% GnP, with these foams presenting a microcellular structure with cell densities above $10^9$ cells/$cm^3$ through the whole range of foaming conditions.

The analysis of the effects of the addition of different amounts of graphene nanoplatelets on the morphology of PC foams made possible a better understanding of how to use the foaming conditions in order to develop low density PC composite foams with tailored cellular morphologies, from microcellular foams to foams with larger and elongated cells, enabling to widen the possible range of applications of these lightweight materials.

**Acknowledgement**

The authors would like to acknowledge the Spanish Ministry of Economy and Competitiveness for the financial support of project MAT2011-26410.

**References**

[1] J. Ling, W. Zhai, W. Feng, B. Shen, J. Zhang, W.G. Zheng, Facile preparation of lightweight microcellular polyetherimide/graphene composite foams for electromagnetic interference shielding, ACS Applied Materials & Interfaces 5 (2013) 2677-2684.

[2] B. Shen, W. Zhai, D. Lu, W. Zheng, Q. Yan, Fabrication of microcellular polymer/graphene nanocomposite foams, Polymer International 61 (2012) 1693-1702.

[3] J. Yang, M. Wu, F. Chen, Z. Fei, M. Zhong, Preparation, characterization, and supercritical carbon dioxide foaming of polystyrene/graphene oxide composites, Journal of Supercritical Fluids 56 (2011) 201-207.

[4] H.-B. Zhang, Q. Yan, W.-G. Zheng, Z. He, Z.-Z. Yu, Tough graphene-polymer microcellular foams for electromagnetic interference shielding, ACS Applied Materials & Interfaces 3 (2011) 918-924.

[5] D. Galpaya, M. Wang, L. Meinan., N. Motta, E. Waclawik, C. Yan, Recent advances in fabrication and characterization of graphene-polymer nanocomposites, Graphene 1 (2012) 30-49.

[6] G. Gedler, M. Antunes, V. Realinho, J.I. Velasco, Novel polycarbonate-graphene nanocomposite foams prepared by $CO_2$ dissolution, IOP Conference Series: Materials Science and Engineering 31 (2012) 012008.

[7] Q. Lan, J. Yu, J. Zhang, J. He, Enhanced crystallization of bisphenol A polycarbonate in thin and ultrathin films by supercritical carbon dioxide, Macromolecules 44 (2011) 5743-5749.

[8] L. Chen, D. Rende, L.S. Schadler, R. Ozisik, Polymer nanocomposite foams, Journal of Materials Chemistry A 1 (2013) 3837-3850.

[9] B. Zhu, W. Zha, J. Yang, C. Zhang, L.J. Lee, Layered-silicate based polystyrene nanocomposite microcellular foam using supercritical carbon dioxide as blowing agent, Polymer 51 (2010) 2177-2184.

[10] G. Gedler, M. Antunes, J.I. Velasco, Graphene-induced crystallinity of bisphenol A polycarbonate in the presence of supercritical carbon dioxide, Polymer 54 (2013) 6389-6398.

[11] L. Chen, L.S. Schadler, R. Ozisik, An experimental and theoretical investigation of the compressive properties of multi-walled carbon nanotube/poly(methyl methacrylate) nanocomposite foams, Polymer 52 (2011) 2899-2909.

[12] M.-T. Liang, C.-M. Wang, Production of engineering plastics foams by supercritical $CO_2$, Industrial & Engineering Chemistry Research 39 (2000) 4622-4626.

[13] J.E. Weller, V. Kumar, Solid-state microcellular polycarbonate foams. I. The steady-state process space using subcritical carbon dioxide, Polymer Engineering & Science 50 (2010) 2160-2169.

[14] J.A.R. Ruiz, J. Marc-Tallon, M. Pedros, M. Dumon, Two-step microcellular foaming of amorphous polymers in supercritical $CO_2$, The Journal of Supercritical Fluids 57 (2011) 87-94.

[15] G. Gedler, M. Antunes, J.I. Velasco, Polycarbonate foams with tailor-made cellular structures by controlling the dissolution temperature in a two-step supercritical carbon dioxide foaming process, The Journal of Supercritical Fluids 88 (2014) 66-73.

[16] V. Kumar, J. Weller, Production of microcellular polycarbonate using carbon dioxide for bubble nucleation, Journal of Engineering for Industry 116 (1994) 413-420.

[17] H.-L. Ma, H.-B. Zhang, X. Li, X. Zhi, Y.-F. Liao, Z.-Z. Yu, The effect of surface chemistry of graphene on cellular structures and electrical properties of polycarbonate nanocomposite foams, Industrial & Engineering Chemistry Research 53 (2014) 4697-4703.

[18] A.V. Nawaby, Z. Zhang, Solubility and diffusivity, in: S.T. Lee (Ed.) Thermoplastic foam processing. Principles and development, CRC Press, London, 2005.

[19] J. Crank, G.S. Park, Methods of measurement, in: J. Crank, G.S. Park (Eds.) Diffusion in Polymers, Academic Press, London, 1968.

[20] Y.W. Cheung, R.S. Stein, Critical analysis of the phase behavior of poly(epsilon-caprolactone) (PCL)/polycarbonate (PC) blends, Macromolecules 27 (1994) 2512-2519.

[21] G. Sims, C. Khunniteekool, Cell size measurement of polymeric foams, Cellular Polymers 13 (1994) 137-146.

[22] R.H. Somani, L. Yang, B.S. Hsiao, Precursors of primary nucleation induced by flow in isotactic polypropylene, Physica A: Statistical Mechanics and its Applications 304 (2002) 145-157.

[23] M.A. Rodríguez-Pérez, R.A. Campo-Arnáiz, R.F. Aroca, J.A. de Saja, Characterisation of the matrix polymer morphology of polyolefins foams by Raman spectroscopy, Polymer 46 (2005) 12093-12102.

[24] F.J. Medellin-Rodriguez, C. Burger, B.S. Hsiao, B. Chu, R. Vaia, S. Phillips, Time-resolved shear behavior of end-tethered nylon 6-clay nanocomposites followed by non-isothermal crystallization, Polymer 42 (2001) 9015-9023.

[25] J.-B. Bao, T. Liu, L. Zhao, G.-H. Hu, X. Miao, X. Li, Oriented foaming of polystyrene with supercritical carbon dioxide for toughening, Polymer 53 (2012) 5982-5993.

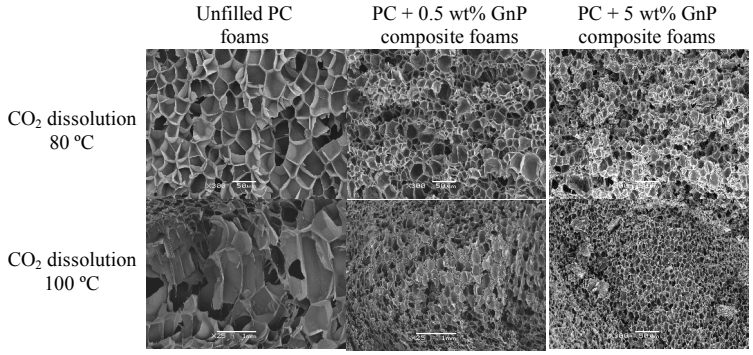
Unfilled PC foams
PC + 0.5 wt% GnP composite foams
PC + 5 wt% GnP composite foams
$CO_2$ dissolution 80 ºC
$CO_2$ dissolution 100 ºC

## Highlights

- Graphene-filled PC foams with tailored morphologies were prepared by $scCO_2$ foaming.
- Graphene addition led to PC foams with higher cell densities than unfilled PC foams.
- At 80 ºC PC-0.5 wt% GnP foams showed a microcellular structure with some larger cells.
- At 100 ºC PC-0.5 wt% GnP foams morphology was fully formed by larger oriented cells.
- The addition of 5 wt% graphene resulted in highly expanded microcellular PC foams.